THE JOURNAL OF PHYSICAL CHEMISTRY A

Article

pubs.acs.org/JPCA

Organic Component Vapor Pressures and Hygroscopicities of Aqueous Aerosol Measured by Optical Tweezers

Chen Cai,[†,‡] David J. Stewart,[‡] Jonathan P. Reid,*[,‡] Yun-hong Zhang,[†] Peter Ohm,[§] Cari S. Dutcher,[§] and Simon L. Clegg[∥]

[†]The Institute of Chemical Physics, Key Laboratory of Cluster Science, Beijing Institute of Technology, Beijing 100081, People's Republic of China

[‡]School of Chemistry, University of Bristol, Bristol, BS8 1TS, U.K.

[§]Department of Mechanical Engineering, University of Minnesota, 111 Church Street SE, Minneapolis, Minnesota 55455, United States

[∥]School of Environmental Sciences, University of East Anglia, Norwich NR4 7TJ, U.K.

Supporting Information

ABSTRACT: Measurements of the hygroscopic response of aerosol and the particle-to-gas partitioning of semivolatile organic compounds are crucial for providing more accurate descriptions of the compositional and size distributions of atmospheric aerosol. Concurrent measurements of particle size and composition (inferred from refractive index) are reported here using optical tweezers to isolate and probe individual aerosol droplets over extended timeframes. The measurements are shown to allow accurate retrievals of component vapor pressures and hygroscopic response through examining correlated variations in size and composition for binary droplets containing water and a single organic component. Measurements are reported for a homologous series of dicarboxylic acids, maleic acid, citric acid, glycerol, or 1,2,6-hexanetriol. An assessment of the inherent uncertainties in such measurements when measuring only particle size is provided to confirm the value of such a correlational approach. We also show that the method of molar refraction provides an accurate characterization of the compositional dependence of the refractive index of the solutions. In this method, the density of the pure liquid solute is the largest uncertainty and must be either known or inferred from subsaturated measurements with an error of <±2.5% to discriminate between different thermodynamic treatments.

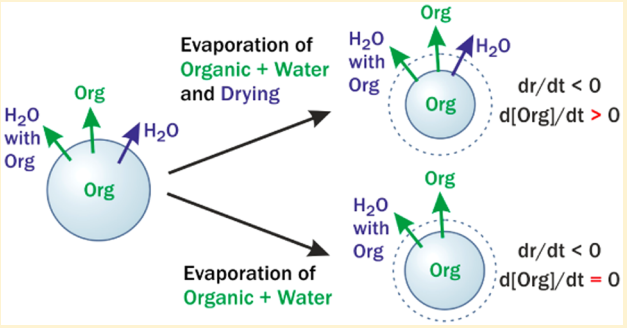

1. INTRODUCTION

The equilibrium partitioning of water and organic components between the gas and condensed phases is critical in determining particle size distributions and compositions in atmospheric aerosol impacting on the tropospheric particulate mass burden, cloud droplet formation, heterogeneous chemistry, and the direct radiative forcing of aerosol.[1−3] Many techniques have been developed to measure changes in the mass of water partitioned to the liquid phase with change in water activity/gas phase relative humidity (RH, see for example refs 4−7). The partitioning of semivolatile organic components between the gas and condensed phases can be inferred from equilibrium state partitioning models, provided values of the pure component vapor pressures of the organic components are known or can be estimated, and subject to the availability of models of the water activity dependent activity coefficients of the organic species.[8,9] Laboratory and field measurements often seek to isolate the changes in gas−particle partitioning of water and (semi-) volatile organic compounds, collectively referred to as S-VOCs below, by assuming that the equilibrium partitioning for S-VOCs and water is approached on considerably different time scales.[10] However, recent simulations of the activation of cloud condensation nuclei (CCN) have reminded us that the two are intimately linked and the cocondensation of both water and water-soluble S-VOCs must be considered to accurately predict cloud droplet number.[11,12]

Hygroscopic growth measurements are frequently reported for submicrometer diameter particles as a change in the wet size of a particle relative to the dry size with variation in RH using a hygroscopic tandem differential mobility analyzer (HTDMA[4]). Alternatively, the relative change in mass or radius of a single particle captured in either an electrodynamic or optical trap can be measured in the laboratory with variation in RH for aerosols of specific composition to provide robust data for equilibrium state models.[13] Pure component vapor pressures of S-VOCs can be measured from bulk phase samples, from ensembles of

Received: October 20, 2014
Revised: December 15, 2014
Published: December 18, 2014

DOI: 10.1021/jp510525r
J. Phys. Chem. A 2015, 119, 704−718

particles, or from single trapped particles.[13−15] Knudsen cell effusion methods are usually restricted to measuring the vapor pressures of bulk phase solid samples.[14] The value for a subcooled liquid, typically required for atmospheric aerosol, must then be inferred using the enthalpy of fusion, the change in heat capacity on melting, and the melting temperature.[14,16,17] Aerosol ensemble and single particle techniques can allow direct access to subcooled liquids and can even permit measurements of vapor pressures on supersaturated aqueous solutions. However, a restricted sensitivity to changes in size over a fixed period of time can often be limiting when performing a measurement, and inferred vapor pressures can be susceptible to fluctuations in environmental conditions (temperature and RH).[18] Indeed, the impact of fluctuations/changes in environmental conditions should be recognized as driving concomitant changes in the gas−particle partitioning of both water and any S-VOC often leading to ambiguity in measurements.[10]

Although measurements of aerosol hygroscopicity and volatility are standard aerosol analyses that are commonly reported, a number of important challenges remain both in performing measurements and in their interpretation. Ensemble measurements of aerosol volatility now commonly represent the volatility of organic components using a volatility basis set derived from measurements at elevated temperatures under dry conditions.[19−25] Reported vapor pressures of even individual semivolatile components measured by different laboratory techniques can vary by more than 4 orders of magnitude.[26] The scarcity of accurate pure component vapor pressures for organic compounds with the low vapor pressures ($<10^{-2}$ Pa) and multifunctionalities representative of atmospheric components limits the validation and improvement of vapor pressure estimation techniques. Barley et al.[10,27,28] have shown that the ambient condensed mass of secondary organic aerosol (SOA) can vary by orders of magnitude dependent on the vapor pressure estimation method used. Indeed, they have also examined the sensitivity of the ambient SOA mass to the degree of nonideality in the solution behavior of organic components when in an aqueous solution droplet. Drying SOA prior to performing a growth measurement using an HTDMA can lead to significant changes in the gas−particle partitioning of S-VOCs and, thus, RH dependent growth curves that can be substantially in error. Indeed, many of the thermodynamic treatments are derived from measurements that attempt to isolate the partitioning of water from S-VOCs leading to models that may depend on data that are not self-consistent. In this brief overview of the challenges faced in characterizing the equilibrium state of aerosol, we have omitted to even mention the possible kinetic limitations that may be imposed on measurements by the formation of amorphous, viscous, or even glassy aerosol,[29−32] and the uncertainty in the value of the mass accommodation/evaporation coefficient.[33,34]

Recently, we have described a new approach for exploring the equilibrium properties of mixed component aqueous aerosol particles using optical tweezers.[18] Rather than attempting to isolate the gas−particle partitioning of water and the S-VOCs in independent measurements, the technique is instead derived from exploiting the intimate coupling between the two. Simultaneous and accurate measurements of the refractive index and size of aqueous aerosol can allow parallel estimations of the change in composition as well as size, providing concurrent information on the gas−particle partitioning of both the S-VOC and water. Conventional measurements instead rely simply on measurements of changes in particle size to measure either the evaporation of an S-VOC or the evaporation/condensation of water.[13] Indeed, rather that attempting to maintain steady environmental conditions (e.g., RH) during measurements of the vapor pressure of an S-VOC, fluctuations in RH are central to the technique, allowing parallel and self-consistent measurements of the equilibrium vapor pressures of S-VOCs and the hygroscopicity of the aerosol. Having previously outlined the framework for performing these measurements, we report new measurements of the hygroscopic growth and vapor pressures of a number of organic components in this publication and compare them with predictions from thermodynamic models. Section 2 provides an overview of the equilibrium state models used to compare with the experimental data. In section 3, we consider some of the inherent uncertainties arising in measurements of the equilibrium behavior of aerosol and consider the sensitivities to key experimental variables, and we briefly summarize the framework used to interpret single particle measurements in section 4. Finally, in section 5 we report equilibrium state measurements for a variety of binary aqueous/organic aerosol droplets.

2. THERMODYNAMIC MODELS

Water and solute activities in liquid mixtures containing water and organic compounds such as the dicarboxylic acids of interest here can be calculated using the universal quasichemical functional-group activity coefficient (UNIFAC) group-contribution method.[35] UNIFAC treats solutions as a mixture of interacting molecular structural groups. The parameters that describe these interactions are determined by fitting to a wide range of vapor−liquid equilibrium and activity data (e.g., Wittig et al., 2003,[36] and references therein). Peng et al.[37] have optimized six of the $a_{i,j}$ UNIFAC energy parameters, using their own measurements of water activities of solutions of seven dicarboxylic acids at room temperature to improve the representation of solvent and solute activities for this class of compounds (see their Figures 1 to 7). In the UNIFAC approach all compounds are assumed to be nondissociating (i.e., there is no treatment of ions). The UNIFAC-Peng equations (i.e., the UNIFAC model with Peng parameters) are used frequently within atmospheric chemical models to estimate the contributions of dicarboxylic acids and other organic compounds to the thermodynamic properties of inorganic−organic acid−water mixtures, for example in the extended AIM aerosol thermodynamic model (E-AIM)[38,39] and the aerosol inorganic−organic mixtures functional groups activity coefficients model (AIOMFAC).[17,40] Thus, it should be noted that references to UNIFAC-Peng calculations below can also be viewed as the results from the AIOMFAC model.

Alternatively, the relationship between water and solute activities and composition can be represented by empirical expressions fitted directly to measurements for the compounds of interest. For example Clegg and Seinfeld[41] have fitted the Redlich−Kister equation[42] to measured water activities of aqueous dicarboxylic acids, including data for solutions supersaturated with respect to the solids. While this approach is highly accurate for the range of concentrations for which there are data (and to which the equation is fitted), extrapolations to higher concentrations and to the pure liquid melt may not be accurate. This extrapolation is important because the activity coefficient of the solute acids relative to a reference state of the pure liquid solute is needed in order to

DOI: 10.1021/jp510525r
J. Phys. Chem. A 2015, 119, 704−718

obtain estimates of the hypothetical vapor pressure of the pure liquid. As an alternative, Dutcher et al. have therefore used a model based upon a multilayer adsorption isotherm,[43,44] which appears to extrapolate particularly well to zero solvent activity (the hypothetical pure liquid solute). The model expresses solute−water interactions in terms of multiple energies of sorption, C_i, where i is the layer number of the adsorbed solvent surrounding the solute molecule. In this work we have fitted the energy of adsorption parameters so that they yield very similar results to the RK predictions over the range of concentrations for which there are experimental data, but extrapolate differently to the pure liquid solute. The results of this model are referred to as "isotherm-RK".

In this work we compare measurements describing the volatility of S-VOCs, and the hygroscopicity of SVOC aerosol droplets, to predictions using both the UNIFAC-Peng and the isotherm-RK models. Figures S1 and S2 in the Supporting Information illustrate the degree of variability between model approaches. In Figure S1 in the Supporting Information, the predicted osmotic coefficient using the UNIFAC-Peng and the isotherm-RK models are compared to experimental data. In Figure S2 in the Supporting Information, we compare concentrations (as mole fraction of solute, x), and activity coefficients of aqueous solutions calculated using the isotherm-RK and UNIFAC-Peng models for malonic acid, and isotherm-PL and E-AIM[37,38] models for sodium chloride. For the isotherm-RK model, the empirical fit parameters for eq 19 in Dutcher et al.[44] are reported in Table 1 for each binary solution

Table 1. Empirical Fit Parameters of Four Different Organic Aqueous Systems

	citric acid	malonic acid	glutaric acid	maleic acid
C1	4.02	0.391	1.67	0.149
C2	0.0524	3.69	0.727	12.8
C3	102	0.0137	0.0132	2.86
C4	0.46	198	2.11	0.0314
C5	0.0479	0.922	46.5	0.248
C6	44.8	0.458	2.45	2.44
C7	1	1	0.0188	48.2
C8	1	1	5.89	0.354

explored in subsequent sections. The large number of fit parameters used here for the isotherm-RK model is an intentional contrast to the fully predictive UNIFAC-Peng treatment. Note, however, that alternative isotherm treatments with only one or two empirical fit parameters, using power law relationships ("isotherm-PL") to describe successive values of the energy of sorption parameters, are also successful in predicting properties within the uncertainty of the available data.[44] Isotherm-PL models are used here only for the isotherm treatment of NaCl and glycerol, which improves the representation of the water activity data for aqueous NaCl over E-AIM, particularly for supersaturated solutions.

3. UNCERTAINTIES IN SINGLE PARTICLE VAPOR PRESSURE MEASUREMENTS

We now assess the uncertainties inherent to measurements of equilibrium state properties, particularly the pure component vapor pressure estimated from evaporation measurements when the evolving size of a particle is the single observable. In particular, we examine the sensitivity of the retrieval of the vapor pressure of an S-VOC to the associated hygroscopic response of the particle. This assessment will be used to provide justification for the new approach used and the recommendation that accurate measurements of both size and composition should be made if many of the challenges in characterizing the equilibrium state of aerosol containing S-VOC are to be addressed. As an S-VOC that has been studied frequently, we use glutaric acid as a benchmark system.

3.1. Oscillations, Drifts, and Fluctuations in Relative Humidity. Monitoring the time evolving size of a single droplet held in an EDB or optical trap is a standard approach from which the vapor pressures of S-VOCs can be inferred or from which the hygroscopic response can be probed. Indeed, vapor pressures are often inferred from measurements with solution droplets in single particle measurements. However, changes in the partitioning of water and the organic component between the condensed and gas phases occur concurrently in any measurement of volatility or hygroscopicity, and isolating one from the other is not always possible.

A simulation of the concerted influence of hygroscopicity and irreversible evaporation of an S-VOC component in driving droplet size change is illustrated in Figure 1. The RH dependence of the equilibrium mass of water partitioned to the particle is calculated from the isotherm-RK model and assumed to be equivalent to the hygroscopicity of glutaric acid throughout. The mass flux of the S-VOC from the solution droplet depends on the RH and size of the droplet and is calculated from an adapted form of the Maxwell equation, accounting for slow diffusional transport of mass away from the particle in the gas phase, as described in our recent publication.[18] Gas diffusion constants for the S-VOC are estimated by the Chapman−Enskog method. Five values for the pure component vapor pressure of the S-VOC have been considered spanning the range 10^{-2} to 10^{-6} Pa; the true value for glutaric acid is $\sim 4.9 \times 10^{-4}$ Pa, but we consider a range of values here to examine the accuracy with which a hypothetical vapor pressure could be measured. Two types of environmental variation occurring on different time scales are included in the simulation: a sinusoidal oscillation in RH with a period (1800 s) and magnitude (±0.5%) typical of those in an air-conditioned laboratory, and short-time Gaussian-limited noise (an instantaneous fluctuation) over a 10 s period with a much finer amplitude (taken as a standard deviation of ±0.5%). These two components have been reported by us as typical in previous measurements. These variations occur about a single mean RH of 75%.

It is clear from the time dependence in radius shown in Figure 1 that size changes driven by hygroscopic response dominate over evaporation of the organic component for all S-VOC volatilities except the very highest when measurements are made over a time scale of a few thousand seconds or less. Even for a droplet containing an S-VOC of vapor pressure of order 10^{-3} Pa, typical of the dicarboxylic acids, simply inferring the vapor pressure from the time-dependent size can lead to significant errors of orders of magnitude, depending on the phase in the RH oscillation during which the vapor pressure is retrieved (see inset for the time dependence of radius). Ambiguity is apparent in interpreting the size change: separating out the S-VOC evaporation from the hygroscopic response is challenging. The accuracy required in the retrieval of droplet size must be at the nanometer level, particularly for droplets containing S-VOCs with vapor pressures of 10^{-4} Pa and lower. Although we use RH cycling here for illustrative purposes, long time drifts over hours typical in laboratory

DOI: 10.1021/jp510525r
J. Phys. Chem. A 2015, 119, 704−718

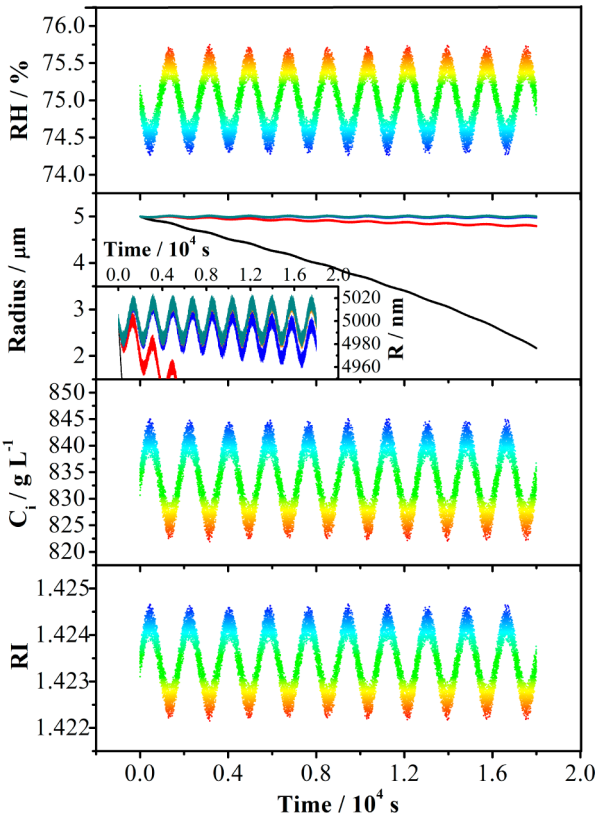

Figure 1. A simulation of the concerted impact of hygroscopic sensitivity and organic component evaporation on the evolving size, solute concentration, and RI of an aqueous S-VOC solution droplet. The RH is set to vary with a sinusoidal time-dependent component and with an additional Gaussian noise component representative of single particle measurements. The color of the lines in the radius/time panel denotes the pure component vapor pressure of the S-VOC: dark cyan, 10^{-6} Pa; orange, 10^{-5} Pa; blue, 10^{-4} Pa; red, 10^{-3} Pa; and black, 10^{-2} Pa. The lowest two vapor pressures are almost superimposed on the scale of this figure, but will be resolved in the correlational analysis in Figure 5. The inset shows an expanded view at early time. The color of the lines in the remaining three panels represents the concentration of the S-VOC in the droplet as defined in the panel showing concentration on a solute molarity scale. The hygroscopic response of the aerosol is taken to be that of glutaric acid.

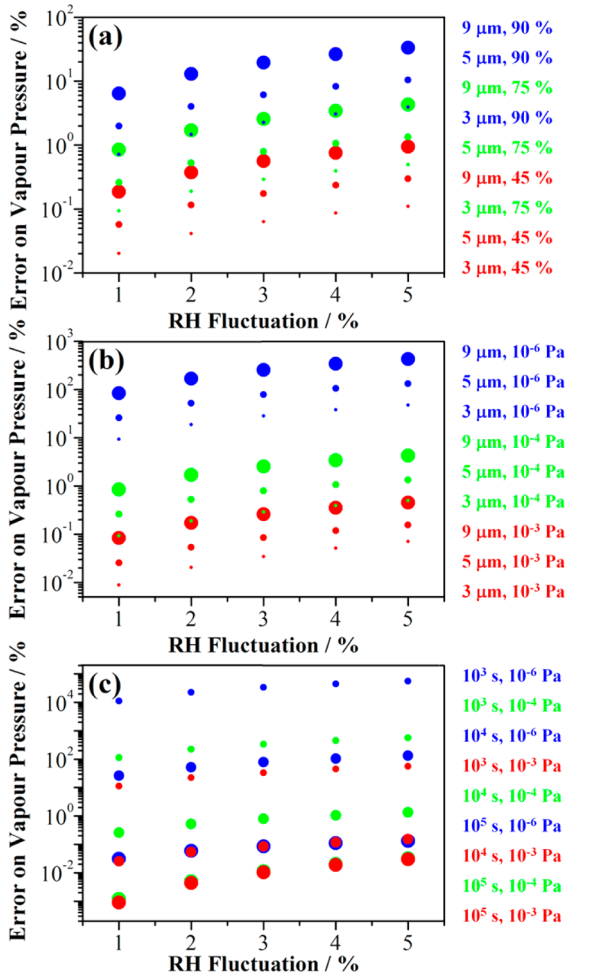

Figure 2. Accuracy in the pure component vapor pressures inferred from evaporation flux measurements with binary aqueous/organic component droplets. The amplitude of fluctuation in the RH on a 10 s time scale is indicated by the *x*-axis. (a) The pure component vapor pressure is 10^{-4} Pa, and the measurement time is taken as 10000 s. The different symbol sizes correspond to droplets of different radii (large to small, 9, 5, and 3 μm, respectively) and the different colors to different RHs (90, 75, and 45% RH are blue, green, and red, respectively). (b) The RH is 75%, and the measurement time is taken as 10000 s. The different symbol sizes correspond to droplets of different radii (large to small, 9, 5, and 3 μm, respectively) and the different colors to different pure component vapor pressures (10^{-6}, 10^{-4}, and 10^{-3} Pa are blue, green, and red, respectively). (c) The RH is 75%, and the droplet radius is 5 μm. The different colors correspond to different pure component vapor pressures (10^{-6}, 10^{-4}, and 10^{-3} Pa are blue, green, and red, respectively), and the symbol sizes correspond to different time periods for the measurement (small to larger, 10^3, 10^4, and 10^5 s, respectively).

environments would similarly lead to errors in estimates of component vapor pressures and would be increasingly problematic, introducing ambiguity when measuring S-VOC fluxes for components with vapor pressures below 10^{-4} Pa. For completeness, we include in Figure 1 the corresponding fluctuations in solution composition (grams of solute per liter of solution, a molarity scale) and droplet refractive index; we will return to the treatments used for these in a later section.

In Figure 1 we have considered one specific set of experimental parameters, a droplet initially of 5 μm radius at a RH of 75% and with a range of S-VOC volatility. The accuracy with which the pure component vapor pressure can be retrieved from such measurements is dependent on each of these quantities. For example, measurements of the vapor pressure of more volatile components are less susceptible to periodic oscillation and long-time drift. We consider the accuracy in the determination of pure component vapor pressure to the droplet size being studied, the RH of the measurement, and the vapor pressure being determined in Figure 2. Numerical values for the errors are given in Table S1 in the Supporting Information. The oscillation in RH is not included in these simulations. Instead, we merely include the Gaussian noise in RH fluctuating on a 10 s time scale with varying amplitude (defined as the standard deviation of the distribution) as indicated. The uncertainty in the fitted slope of the simulated time dependence of size, including the "noise" from the RH fluctuations, is then used to infer the upper and lower limits on the vapor pressure, and these are compared to the value of the vapor pressure used to simulate the time-dependent trends, leading to an estimate of the percentage error in vapor pressure.

DOI: 10.1021/jp510525r
J. Phys. Chem. A 2015, 119, 704−718

The accuracy of the retrieved vapor pressure for a component of vapor pressure 10^{-4} Pa from simulations of droplets of different size and at different RH is considered in Figure 2a. Substantially higher errors are incurred in estimated S-VOC vapor pressure when measurements are made at high RH due to the much larger size changes driven by hygroscopic response. Larger fluctuations in RH lead to larger errors in vapor pressure determinations, and measurements must be performed over a longer period of time to resolve a change in size due to volatilization of the S-VOC. Further, provided we assume that the droplet size can be determined with unlimited accuracy, more accurate retrievals of vapor pressure result when measurements are made on smaller droplets. An instant recommendation from Figure 2a is that measurements should be made on droplets smaller than 5 μm in radius if the error in the vapor pressure determination is to be below ±10% over the full RH range over a 10000 s measurement period. We have also considered the uncertainties in retrieved vapor pressures arising from systematic errors and fluctuations in temperature. Given the accuracy of temperature measurements, these uncertainties are extremely small when compared to those that arise from RH drifts and fluctuations. However, for completeness we include the results of the uncertainty analysis in Figure S4 in the Supporting Information.

The estimated errors in vapor pressure can be compared with the uncertainties in our previous EDB and optical tweezers measurements of the vapor pressures of malonic and glutaric acid.[45] At typical RHs and droplet radii (3−4 μm) of optical tweezers measurements, even at as high an RH as 90%, the uncertainty in the slope of the time dependence of the mass of S-VOC in the droplet is $\ll\pm$0.5% when the RH variation is within ±0.2%. For a single droplet measurement, this corresponds to an error in retrieved vapor pressure of $\ll$1%, consistent with Figure 2a. It should be noted that this does not consider reproducibility between measurements on different droplets, but only represents the error for a single measurement on a single particle.

At an intermediate RH of 75%, the influence of RH fluctuations on the error in the vapor pressure measurement increases as the pure component vapor pressure decreases from 10^{-3} to 10^{-4} and 10^{-6} Pa, Figure 2b. Again, the measurement period is defined as 10000 s. Errors can exceed 100% when measuring vapor pressures of 10^{-6} Pa on coarse mode particles, particularly when larger than 9 μm radius, typical of EDB measurements. This severely limits the accuracy of single particle techniques for measuring the vapor pressures of low volatility organic compounds, the very compounds that are most likely to partition to the condensed phase entirely in the atmosphere and for which values are required. At 75% RH, measuring vapor pressures in excess of 10^{-3} Pa should have an accuracy of $\ll\pm$1% under all possible measurement conditions.

Clearly, to measure vapor pressures of 10^{-5} Pa or lower, the time of the measurement must be increased for accurate measurements to be made; the dependence of the error in vapor pressure retrieval on the duration of the measurement is considered in Figure 2c. To reduce the uncertainty to <±10% for a component vapor pressure of 10^{-6} Pa using a 5 μm radius droplet at 75% RH requires that the measurement be made over a time $\gg$10000 s. However, it must be remembered that measurements over such long time frames become susceptible to long-term drift in the environmental conditions, such as temperature, introducing new errors into the measurement.

3.2. Systematic Inaccuracies in RH Determination. Not only can the RH oscillate about a mean value or fluctuate on a short time scale, but the actual measurement of RH may be systematically in error due to inaccuracies in probe response or calibration. We have shown previously that the retrieval of the refractive index of an optically tweezed aerosol droplet can allow extremely accurate measurements of the RH that the droplet is equilibrated with, typically <±0.1%.[46,47] Based on the relationship of refractive index to mass fraction of solute and, thus, water activity (see later for a detailed discussion), correlation plots of the form shown in Figure 3a can be derived. The accuracy of using the droplet RI to determine water activity is partly dependent on the accuracy of the thermodynamic treatment used to relate mass fraction of solute to water activity. However, even though the droplet RI is typically determined with an accuracy as good as ±0.05%, the RI accuracy remains the limiting factor governing the uncertainty in the retrieved RH as the thermodynamic treatments are considerably more accurate.[47] Measurements of RH have been performed both with trapped aqueous sodium chloride and aqueous glutaric acid droplets and a typical capacitance RH probe, calibrated independently prior to the measurement. The data shown in Figure 3a is intended only to be representative, but indicates that typical systematic errors of ±2% or larger can result when a typical capacitance probe is used and the error is RH dependent, consistent with the stated accuracy of such hygrometers.

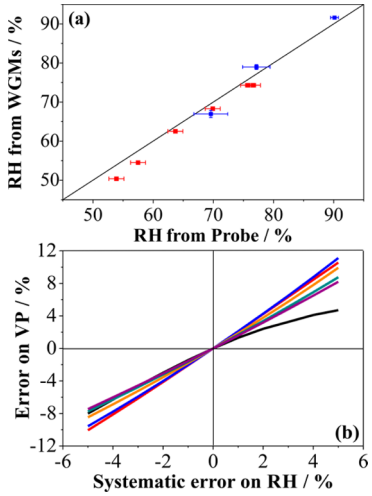

Figure 3. (a) (a) Consistency between RH determined by a capacitance probe and from the RI determined for aqueous NaCl (red) and glutaric acid (blue) droplets from fitting the characteristic whispering gallery modes in the Raman fingerprint. (b) Error incurred in the estimation of the pure component vapor pressure due to systematic errors in the RH. The model system chosen is, once again, an aqueous glutaric acid droplet. Different colors represent different RHs: 90% (black), 80% (red), 70% (blue), 60% (orange), 50% (dark cyan), 40% (navy).

We consider the error in the inferred pure component vapor pressure resulting from systematic errors in RH in Figure 3b for an aqueous glutaric acid droplet. A systematic error in the water activity translates into a systematic error in the mass fraction of solute in the droplet and in the activity coefficients then used to infer the pure component vapor pressure. As suggested above, typical errors in RH may be ±2% although these only lead to errors in the estimated vapor pressures in the range ±10%,

DOI: 10.1021/jp510525r
J. Phys. Chem. A 2015, 119, 704−718

smaller than the errors arising from fluctuations and drifts in the RH discussed above.

3.3. Uncertainties in Determination of Droplet Size. As suggested by the discussion of Figure 1, measurements of the vapor pressures of low volatility S-VOCs require extremely accurate measurements of size. In Figure 4 (Table S2 in the Supporting Information), we consider how the uncertainty in the size measurement limits the accuracy with which pure component vapor pressures can be determined when the evolving size is measured over a time window of 10000 s. For a 5 μm radius droplet, uncertainties in radius measurement of $\pm$0.05, 0.5, 2, and 5% correspond to uncertainties of 2.5, 25, 100, and 250 nm, respectively. While the lowest value corresponds to the uncertainty in droplet size from an aerosol optical tweezers measurement using cavity enhanced Raman spectrum,[48] the upper limit is more comparable to the level of error in an elastic light scattering phase function measurement of size used in an EDB or Bessel beam trap.[49−51] A random Gaussian distribution in the size determination is imposed on the size in a similar manner as the fluctuation in RH in Figure 1.

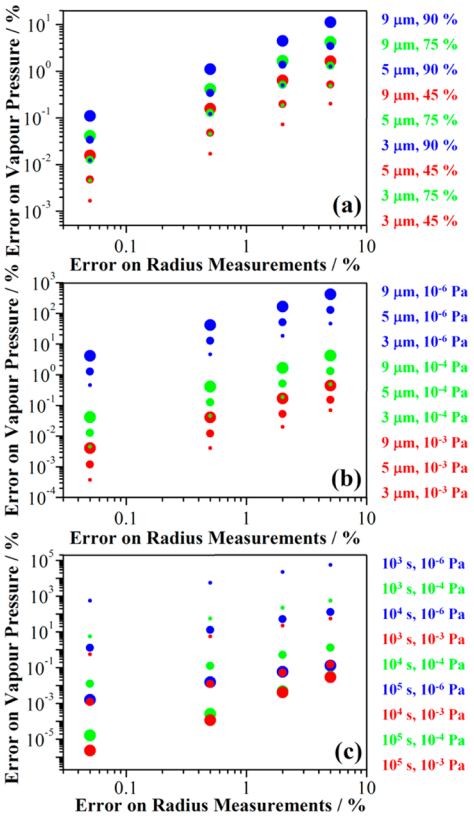

Figure 4. Sensitivity of estimation of pure component vapor pressure to the uncertainty in the measurement of particle size. The uncertainty in size is assumed to be a random uncertainty (white noise) with a standard deviation as indicated by the *x*-axis as a percentage. (a) The pure component vapor pressure is 10^{-4} Pa, and the evolving size is simulated for 10000 s. The different symbol sizes correspond to droplets of different radii (large to small, 9, 5, and 3 μm, respectively) and the different colors to RHs (90, 75, and 45% RH are blue, green, and red, respectively). (b) The RH is 75%, and the evolving size is measured for 10000 s. The different symbol sizes correspond to droplets of different radii (large to small, 9, 5, and 3 μm, respectively) and the different colors to different pure component vapor pressures (10^{-6}, 10^{-4}, and 10^{-3} Pa are blue, green, and red, respectively). (c) The RH is 75%, and the droplet radius is 5 μm. The different colors correspond to different pure component vapor pressures (10^{-6}, 10^{-4}, and 10^{-3} Pa are blue, green, and red, respectively), and the symbol sizes correspond to different time periods over which the evaporation is measured (small to large, 10^3, 10^4, and 10^5 s, respectively).

When measuring the vapor pressure of an S-VOC of volatility 10^{-4} Pa, larger uncertainties in size retrieval will obviously lead to larger errors in the estimation of the vapor pressure, as shown in Figure 4a. Smaller vapor pressures require more accurate measurements of size to make measurements of small size changes over the same time frame. Further, if the percentage error in size is consistent across all droplet sizes, measurements of evaporation from smaller droplets are more accurate. Smaller errors are incurred when measuring vapor pressures at lower RH due to the increased evaporative flux of the S-VOC when the droplet has a higher mass fraction of solute. At an intermediate RH of 75%, Figure 4b, the error in the vapor pressure arising from the uncertainty in size exceeds $\pm$10% only for measurements of vapor pressures of 10^{-6} Pa and less when the error in the size measurement is $>\pm$0.5%.

Clearly, measurements must be made over longer time intervals if the error in radius is large, as shown in Figure 4c. For an uncertainty in radius of $\pm$5%, measurements made over 10^4 s lead to an uncertainty of $>\pm$100% for all vapor pressures considered, and consequently measurements should instead be made over a time period $\gg 10^4$ s. However, it should also then be remembered that slow drifts in the environmental conditions can impose significantly restrictions on making such long time frame measurements.

3.4. Nonzero Background of Evaporating S-VOC. Evaporation flux measurements either from single particles or from ensembles can be severely compromised by a background level of the evaporating S-VOC that is not zero. This can be a significant issue if measurements are made of a volatile component from an ensemble of particles or if the gas flow rate through the cell containing a single trapped particle is not sufficient to remove the evaporating component. The presence of a background level of the evaporating S-VOC leads to a diffusional concentration gradient from the surface of the aerosol droplet into the gas phase that is artificially lower than it would otherwise be. The elevation of the background level of the S-VOC leads to a suppression in the mass flux of S-VOC from an aerosol droplet and the estimation of a vapor pressure that is systematically low. Again for the case of glutaric acid, the underestimate of the vapor pressure that would be retrieved if the background concentration of glutaric acid were elevated up to 15% of its pure component value is shown in Figure S3 in the Supporting Information for measurements over a range of RHs. Greater error is incurred when measurements are performed at higher RH due to the lower mass fraction of solute in the droplet and the lower vapor pressure above the solution. Notably, this error can also be significant and can lead to errors of an order of magnitude or more in the estimated value of the pure component vapor pressure if the elevation in the background level of the S-VOC exceeds 10% of the pure component value.

4. CORRELATIONAL FRAMEWORK FOR AEROSOL OPTICAL TWEEZERS MEASUREMENTS

The challenges of achieving the required stability in environmental conditions and accuracy in determination of droplet size have been described in section 3. Instabilities in RH and inaccuracies in the determination of droplet radius can lead to substantial errors in the estimation of S-VOC vapor pressures,

DOI: 10.1021/jp510525r
J. Phys. Chem. A 2015, 119, 704−718

particular if the vapor pressure is 10^{-4} Pa or lower. Long experiments are required on individual droplets, introducing additional complications such as contamination by species (e.g., ammonia) within any gas flow. Measurements at high RH are particularly challenging even though it is frequently desirable to map out the solution vapor pressures over a wide range in RH in order to validate models of the activity coefficients of the organic components within the aerosol as well as the activity coefficient of water. Direct measurements of the evolving composition of the aerosol as well as the size are highly desirable if accurate measurements of droplet hygroscopicity and S-VOC vapor pressures are to be achieved.

We have recently shown that simultaneous measurements of the evolving size and RI of aqueous optically tweezed aerosol can be achieved with high accuracy, <±0.05% in both cases.[46,48] From the RI, the composition of the aerosol can be inferred. Given that the variations in size and composition can be attributed to changes in the partitioning of water and any semivolatile components between the particle and the gas phase, changes in water partitioning due to hygroscopic response (leading to changes in refractive index) can be conveniently separated from changes in water and S-VOC partitioning due to the evaporation/condensation of the S-VOC component (with no associated change in RH and RI). Thus, the hygroscopicity and vapor pressures of S-VOCs can be inferred from a time series of both size and refractive index. Indeed, rather than attempting to achieve the high stability in environmental conditions that is required if just the size is measured, this new approach relies on short time fluctuations in RH and long-term trends in size and composition to resolve the changes occurring due to water and S-VOC partitioning.

We have described the framework for analyzing the correlated changes in droplet size and refractive index in detail in ref 18 and refer the reader to this publication. In brief, from a time series of radius, r, and composition measurements, such as that shown in Figure 1, we have demonstrated that a correlational analysis can be used to estimate the water activity dependence of the solute concentration and the vapor pressure of the S-VOC. More specifically, the Maxwell equation,[13,45,52,53]

$$\frac{dm_{org}}{dt} = \frac{4\pi r M_{org} D_{org,gas}}{RT} \Delta p_{org} \quad (1)$$

can be written in the form

$$r^2 \frac{dC_{org}}{dt} = \frac{3 M_{org} D_{org,gas}}{RT} \Delta p_{org} - 3 C_{org} r \frac{dr}{dt} \quad (2)$$

C_{org} is defined as the solution phase concentration of the S-VOC (kg m^{-3}) in the multicomponent droplet, equivalent to the density of the organic liquid in a single component droplet. The mass flux of the organic component depends on the difference between the vapor pressure of the organic component at the droplet surface ($p_{org,r}$) and the partial pressure at infinite distance ($p_{org,\infty}$); this is written as Δp_{org}. In most experimental determinations of vapor pressures, the background partial pressure at infinite distance can be assumed to be 0. M_{org} and $D_{org,gas}$ are the molar mass and diffusion coefficient[54−58] of the organic component in the gas phase, respectively. In multicomponent droplets, such as the aqueous binary solutions investigated in this study, the equilibrium vapor pressure of the organic component at the droplet surface is related to the vapor pressure of the pure liquid organic by

$$p_{org,r} = p^{o}_{org} x_{org} \gamma_{org} \quad (3)$$

where x_{org} and γ_{org} are the mole fraction of the organic species in solution and the mole fraction activity coefficient relative to the pure liquid reference state, respectively. Then, in this form, a graph of $r^2\, dC_{org}/dt$ against $r\, dr/dt$ is linear with gradient and intercept, which allows the determination of the hygroscopic response (solute concentration at a particular RH) and vapor pressure of the organic component. Specifically,

$$\text{gradient of correlational plot} = -3C_{org} \quad (4)$$

$$\text{intercept of correlational plot} = \frac{3 M_{org} D_{org,gas}}{RT} \Delta p_{org} \quad (5)$$

It should be noted that including the radius scaling in the ordinate and abscissa allows data to be directly compared for droplets of differing size.

Correlational plots of the transient gradients in radius and solute concentration for all simulations shown in Figure 1 are presented in Figure 5, with transient gradients taken at each

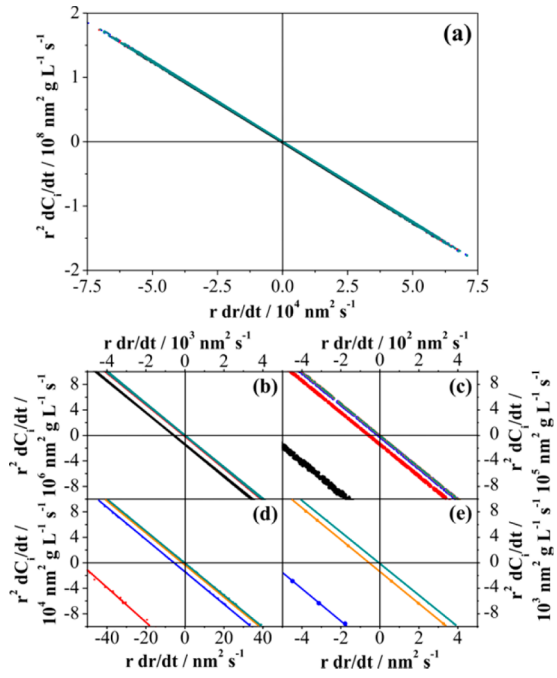

Figure 5. Correlation plots of the instantaneous gradient in concentration and squared radius for the simulations shown in Figure 1. Panel a shows the correlation for all simulations. Panels b−e show increasingly expanded views of the correlations, indicating the intercepts for components of decreasing vapor pressure. The different colors represent different pure component vapor pressures as defined in Figure 1.

time over the neighboring ±10 s of data (in this case simulated data). While panel a shows the correlation over all of the entire data sets, panels b−d show progressively expanded views around the intercepts. As suggested above, the y-intercept allows the vapor pressure to be determined with extremely high accuracy, even down to 10^{-6} Pa for the simulations presented in Figure 1. It should be noted that if size alone were to be recorded in these measurements, the size changes due to evaporation of the S-VOCs over 10000 s would be 1229.2, 117.1, 11.2, 1.1, and 0.1 nm for the droplets containing components of vapor pressures 10^{-2} Pa, 10^{-3} Pa, 10^{-4} Pa, 10^{-5}

DOI: 10.1021/jp510525r
J. Phys. Chem. A 2015, 119, 704−718

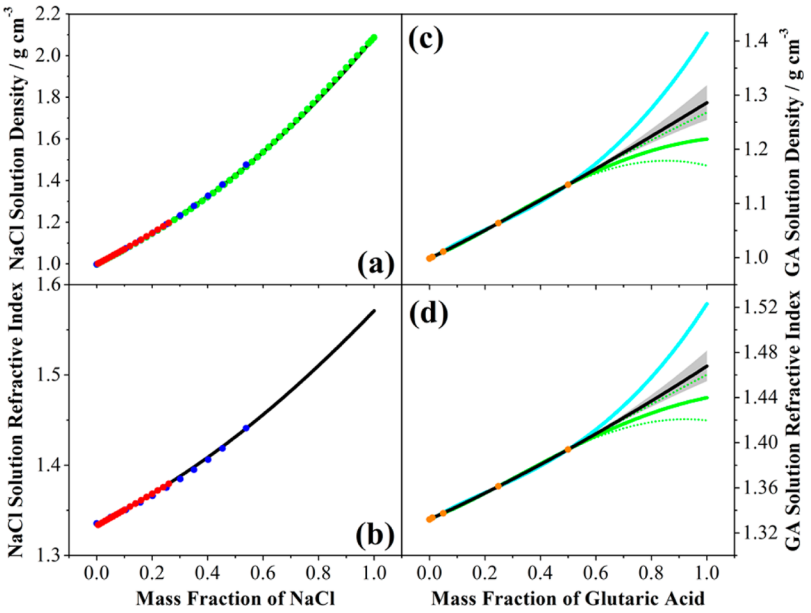

Figure 6. Dependence of the density (a, c) and RI (b, d) of aqueous sodium chloride (a, b) and glutaric acid (c, d) solutions on the mass fraction of solute. Circles are from bulk measurements (blue, measurements by Tang;[64] red, CRC handbook;[70] orange, Soonsin et al.[66]). The green symbols in panel a are from Clegg et al.[62] The black lines represent the fits to the subsaturation density data and the estimated refractive index from the molar refraction mixing rule. The gray envelope indicates the uncertainty in refractive index and density assuming an uncertainty in the pure component density of ±2.5% in the unconstrained fit. In panel c, the cyan line is the density fit constrained to the crystalline value at an mfs of 1 and the green line is the fit constrained to the prediction using the method of Girolami with associated uncertainty of ±0.049 g cm^{-3} (indicated by the dashed green lines).

Pa, and 10^{-6} Pa, respectively. All of the simulated time-dependencies show the same gradient in Figure 5 as the hygroscopic response was assumed to be that of glutaric acid throughout. If measurements were performed around a sequence of widely varying set RH values, a different gradient would be apparent in the correlation plot for each RH from which the variation in solute concentration with RH can be retrieved. We now apply this framework in the determination of component vapor pressures

5. AEROSOL OPTICAL TWEEZERS MEASUREMENTS OF VAPOR PRESSURES AND HYGROSCOPICITIES

5.1. Experimental Description. The aerosol optical tweezers system, including the application of Raman spectroscopy to determine particle size and refractive index, has been described in detail previously[47,59,60] and will be only briefly summarized here. The optical trap is formed by focusing light from a solid-state Nd:YVO_4 laser, frequency doubled to give a wavelength of 532 nm, through a 100× oil immersion objective (numerical aperture of 1.25). The tightly focused beam exerts a gradient force on any aerosol droplet drifting into the focal volume; a cloud of aerosol is introduced to the trapping cell from a medical nebulizer (Omron MicroAIR Pocket Nebulizer). Typical droplets with diameters between 4 and 20 μm can be captured with laser powers of 5−15 mW. A blue LED provides illumination for recording an image by conventional bright-field microscopy. The laser and LED illumination wavelengths are removed from the backscattered Raman signal from the droplet by appropriate notch and long pass filters, before being focused through the entrance slit of a 0.5 focal length spectrograph. The Raman scatter is dispersed by a 1200 grooves/nm grating and the wavelength resolved spectrum recorded by a CCD array of 1024 × 256 pixels. The spectroscopic time resolution is 1 s. The broad underlying

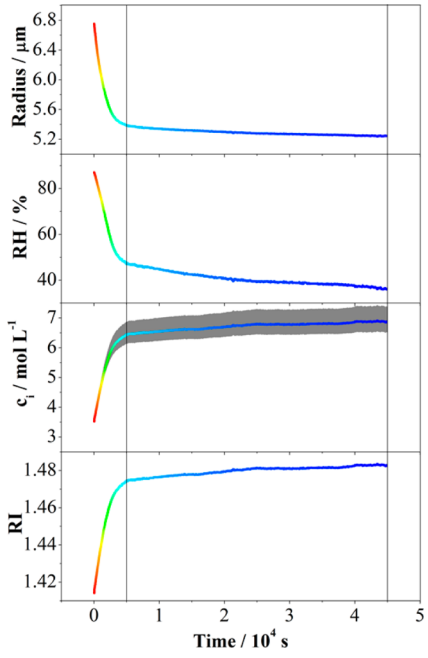

Figure 7. Time dependence in droplet radius, RH (direct measurement from capacitance probe), solute concentration, and RI for a typical measurement with aerosol optical tweezers for an aqueous citric acid droplet (different colors represent different RH). The gray envelope on the estimated composition shows the sensitivity of the compositional retrieval to ±2.5% uncertainty in the pure solute density for citric acid.

spontaneous Raman bands can be used to confirm the presence of organic components and estimate the solute concentration. In addition, stimulated Raman scattering occurs at wavelengths commensurate with whispering gallery modes (WGMs)

DOI: 10.1021/jp510525r
J. Phys. Chem. A 2015, 119, 704−718

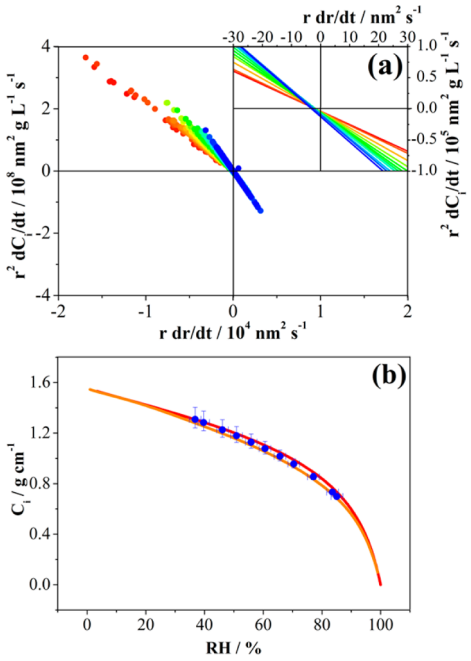

Figure 8. (a) Examples of correlation plots from hygroscopicity data recorded for an aqueous citric acid droplet for the data shown in Figure 9 with the same color gradation. (b) The hygroscopic growth curve (RH−concentration) derived from the correlational analysis for the data set in panel a (blue points). Measurements are compared with predictions from the isotherm-RK model (orange line) and UNIFAC-Peng model (red line). The gray envelope on the estimated composition in Figure 7 is indicated by the *y*-error bar in the measured values.

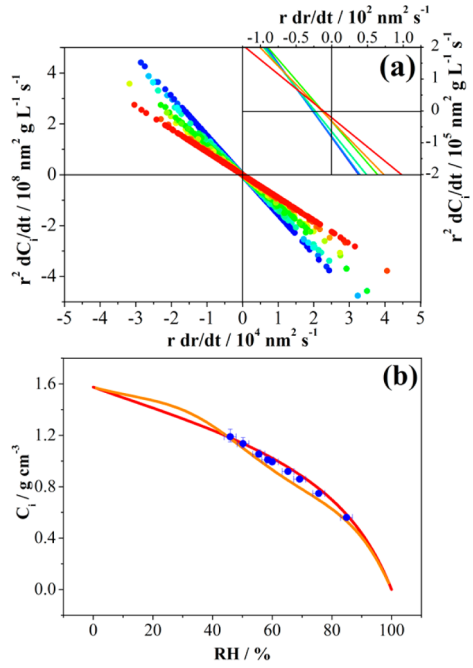

Figure 10. (a) Examples of correlation plots from hygroscopicity data recorded for an aqueous malonic acid droplet for the data shown in Figure 9. (b) The hygroscopic growth curve (RH−concentration) derived from the correlational analysis for the data set in panel a (blue points). Measurements are compared with predictions from the isotherm-RK model (orange line) and UNIFAC-Peng model (red line). The gray envelope on the estimated composition in Figure 9 is indicated by the *y*-error bar in the measured values.

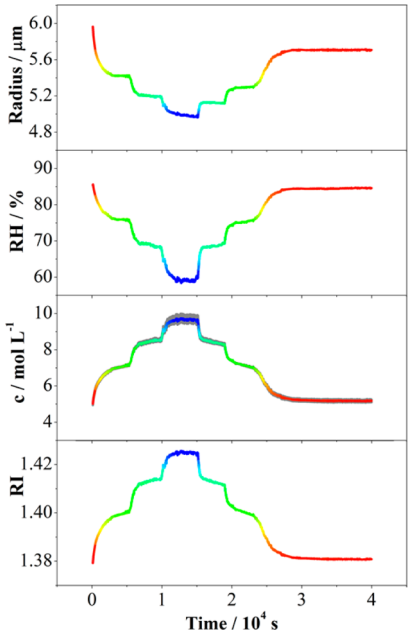

Figure 9. Time dependence in droplet radius, RH (direct measurement from capacitance probe), solute concentration, and RI for a typical measurement with aerosol optical tweezers for an aqueous malonic acid droplet (different colors represent different RH). The gray envelope on the estimated composition shows the sensitivity of the compositional retrieval to ±2.5% uncertainty in the pure solute density for malonic acid.

superimposed on the spontaneous bands. The unique fingerprint that results can be used to estimate both the size and composition of the droplet with high accuracy by comparing the observed WGM wavelengths with predicted wavelengths from Mie scattering calculations.[46] The droplet size and refractive index can be in principle determined with uncertainties of ±2.2 nm and ±0.00065, respectively, based on numerical simulations.[48] Uncorrelated fluctuations from successive frames provide a measure of the errors associated with the fitting rather than the real fluctuations that occur as a result from fluctuations in RH over a longer time scale. Uncertainties of ±5.0 nm and ±0.00061 in refractive index are typical over a period of 10 s for the measurements presented here. Then, gradients associated with the fluctuations in size and composition are calculated between successive 10 s steps from the averaged size and composition over ten 1 s data points.

The RH experienced by the trapped aerosol droplet is varied by adjusting the ratio of dry nitrogen gas flow and a nitrogen gas flow humidified by passing through a bubbler containing deionized water. The mass flow rate of each flow is controlled by a needle valve and displayed by flow meters (MKS, U.K.). The RH of the gas flow is monitored by capacitance probes (Honeywell HIH 4602), one before and a second after the sample cell. The total mixed gas flow rate introduced into the cell was kept constant at 100 cm^3 min^{-1}; only the proportions of humidified and dry flows were varied. To infer the hygroscopicity and component vapor pressure from the correlation approach, the RH is varied over as wide a range as practicable, usually up to 90% and below 40% or as low as possible without the droplet undergoing crystallization. The

DOI: 10.1021/jp510525r
J. Phys. Chem. A 2015, 119, 704−718

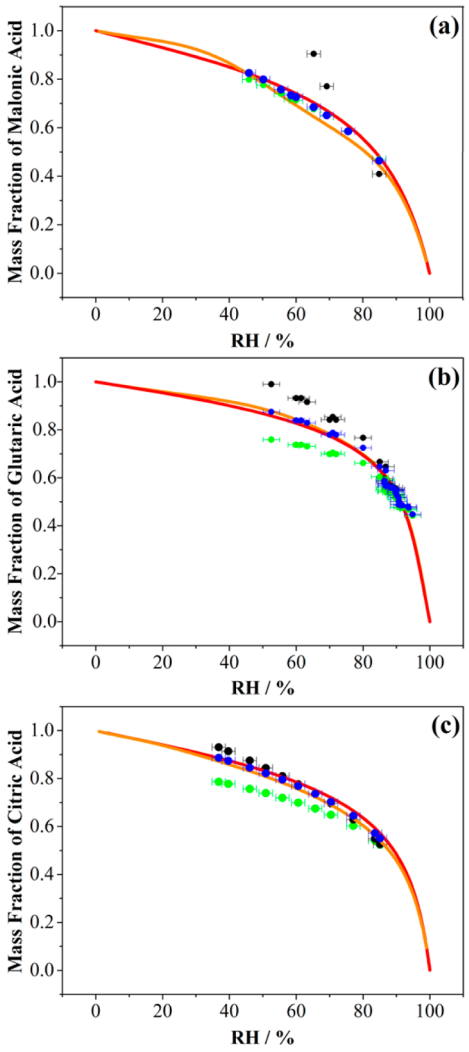

Figure 11. Hygroscopicity curves of experimental measurements compared with predictions from the isotherm-RK model (orange line) and UNIFAC-Peng model (red line). The three symbol colors correspond to different treatments of the pure component density: constrained to subsaturated values alone (blue points), constrained also to the crystalline value at an mfs of 1 (green points), and constrained to the value of the Girolami at an mfs of 1 (black points). (a) Malonic acid, (b) glutaric acid, and (c) citric acid.

RH may be decreased/increased in steps or change more gradually with typical time scales to effect an RH change of 100 s. The chemicals were purchased from Sigma-Aldrich with high purity (≥99%) and were used without further purification.

5.2. The Estimation of Droplet Solution Composition from Measurements of Refractive Index. Although the refractive index can be retrieved with high accuracy from optical tweezers measurements, we must consider the accuracy with which the composition (in units of solute molarity for use in the correlation analysis) can be inferred. Although a number of mixing rules for estimating the refractive indices of mixed component solutions have been used routinely, the method of molar refraction provides a self-consistent treatment for predicting both the solution density and refractive index from their relationship through the Lorentz−Lorenz equation.[61] This method will be used here. From predictions of the dependence of solution density and refractive index on mass fraction of solute, the dependence of the refractive index on solute

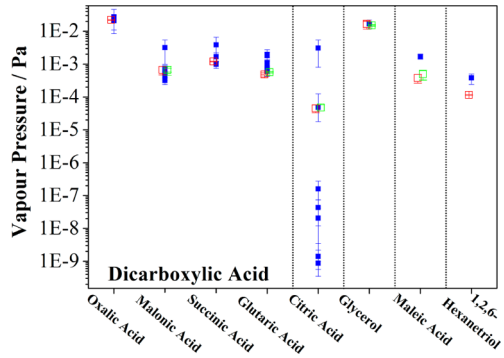

Figure 12. Summary of all previous literature values of pure component vapor pressures inferred from different organic/aqueous systems. Results from this study using the UNIFAC-Peng model to estimate solute activity are shown by the red points and using the isotherm-RK model are shown by the green points. Previously reported values are shown by the blue plots.

molarity can be inferred. Then, the refractive index retrieved in the measurement at any point in time can be converted directly into a value of the solute molarity, as indicated in Figures 1 and S2 in the Supporting Information.

On a mole fraction basis, the molar refraction of a solution, R_e, can be calculated from the molar refractions of the individual components, R_i, and the mole fractions, x_i.[61] For a solution containing N components

$$R_e = \sum_{i=1}^{N} x_i R_i \tag{6}$$

The molar refraction of component i can be estimated from the refractive index, n_i, molar mass, M_i (g mol^{-1}), and mass density, ρ_i (g cm^{-3}), of component i in its pure form. More specifically,

$$R_i = \frac{M_i}{\rho_i}\left(\frac{n_i^2 - 1}{n_i^2 + 2}\right) \tag{7}$$

A similar expression relates the molar refraction of the solution to the effective molar mass, M_e, of the solution and the density of the solution, where

$$M_e = \sum_{i=1}^{N} x_i M_i \tag{8}$$

From the equations presented so far, the molar refraction of the solution, and thus the refractive index, can be estimated accurately as a function of the mole fractions of solutes and the molar masses of the solutes, provided the densities and refractive indices of the pure solutes are known and assuming the density of the solution as a function of mole fraction can be measured. It should be noted that the conversion between mole fraction and mass fraction of solute (mfs) is trivial and we will use the two interchangeably. If volume additivity is assumed, the density of the solution can in fact be estimated from the densities of the pure components and the mole fractions alone. In this case, the only quantities needed to predict the solution densities and refractive indices of the full range of solution compositions are the pure component values. However, the volume additivity approach breaks down for real solutions where interactions between solutes can be significant.[62]

To avoid the assumption of volume additivity to estimate solution density, a parametrization of solution density as a

DOI: 10.1021/jp510525r
J. Phys. Chem. A 2015, 119, 704−718

Table 2. Literature Data for Vapor Pressures of SVOCs Reported in This Study

C_n	name	p°_{org}/Pa	error(+)/Pa	error(−)/Pa	T/K	refs
2	oxalic acid	2.22×10^{-2}	5.55×10^{-4}	5.55×10^{-4}	298	this study
		2.74×10^{-2}	1.90×10^{-2}	1.90×10^{-2}		Booth et al. 2010[14]
		2.10×10^{-2}	1.00×10^{-2}	1.00×10^{-2}		Booth et al. 2010[14]
3	malonic acid	6.61×10^{-4}	1.92×10^{-4}	1.92×10^{-4}	298	this study (UNIFAC-Peng)
		6.58×10^{-4}	8.79×10^{-5}	2.00×10^{-4}		this study (isotherm-RK)
		3.19×10^{-3}	2.20×10^{-3}	2.20×10^{-3}		Booth et al. 2010[14]
		4.90×10^{-4}	1.00×10^{-4}	1.00×10^{-4}		Riipinen et al. 2007[65]
		6.75×10^{-4}	2.25×10^{-4}	2.25×10^{-4}		Pope et al. 2010[45]
		4.90×10^{-4}	1.23×10^{-4}	1.23×10^{-4}		Riipinen et al. 2007[65]
		3.20×10^{-4}	8.00×10^{-5}	8.00×10^{-5}		Zardini et al. 2009[7]
		4.30×10^{-4}	1.08×10^{-4}	1.08×10^{-4}		Soonsin et al. 2010[66]
		7.30×10^{-4}	1.83×10^{-4}	1.83×10^{-4}		Koponen et al. 2007[67]
4	succinic acid	1.20×10^{-3}	3.00×10^{-5}	3.00×10^{-5}	298	this study
		3.86×10^{-3}	2.70×10^{-3}	2.70×10^{-3}		Booth et al. 2010[14]
		1.70×10^{-3}	5.00×10^{-4}	5.00×10^{-4}		Soonsin et al. 2010[66]
		9.90×10^{-4}	2.48×10^{-4}	2.48×10^{-4}		Koponen et al. 2007[67]
5	glutaric acid	4.85×10^{-4}	7.30×10^{-5}	1.80×10^{-5}	298	this study (UNIFAC-Peng)
		5.67×10^{-4}	3.41×10^{-5}	1.88×10^{-5}		this study (isotherm-RK)
		1.96×10^{-3}	4.00×10^{-4}	4.00×10^{-4}		Booth et al. 2010[14]
		9.30×10^{-4}	2.80×10^{-4}	2.80×10^{-4}		Soonsin et al. 2010[66]
		7.10×10^{-4}	1.78×10^{-4}	1.78×10^{-4}		Koponen et al. 2007[67]
		1.08×10^{-3}	2.70×10^{-4}	2.70×10^{-4}		Pope et al. 2010[45]
		6.10×10^{-4}	1.80×10^{-4}	1.80×10^{-4}		Bilde and Pandis 2001[68]
		1.80×10^{-3}	9.60×10^{-4}	4.70×10^{-4}		Ribeiro da Silva et al. 1999[69]
"3"	glycerol	1.66×10^{-2}	4.93×10^{-3}	3.47×10^{-3}	298	this study (UNIFAC-MP*)
		1.51×10^{-2}	1.05×10^{-3}	4.93×10^{-4}		this study (isotherm-PL*)
		1.68×10^{-2}	5.05×10^{-3}	5.05×10^{-3}		CRC Handbook[70]
"4"	maleic acid	3.74×10^{-4}	1.09×10^{-4}	1.10×10^{-4}	298	this study (UNIFAC-Peng)
		4.88×10^{-4}	1.49×10^{-4}	1.66×10^{-4}		this study (isotherm-RK)
		1.71×10^{-3}	3.00×10^{-4}	3.00×10^{-4}		Winstrom et al. 1949[71]
"5"	citric acid	4.50×10^{-5}	1.19×10^{-5}	1.19×10^{-5}	298	this study (UNIFAC-Peng)
		4.80×10^{-5}	9.64×10^{-6}	9.64×10^{-6}		this study (isotherm-RK)
		3.10×10^{-3}	2.30×10^{-3}	2.30×10^{-3}		Booth et al. (liquid) 2010[14]
		4.79×10^{-5}	7.70×10^{-5}	3.00×10^{-5}		Booth et al. (solid) 2010[14]
		2.05×10^{-8}	1.95×10^{-8}	1.95×10^{-8}		Yaws et al. 2009[72]
		8.70×10^{-10}	1.31×10^{-9}	5.20×10^{-10}		Compernolle et al. 2011[73]
		1.40×10^{-9}	2.11×10^{-9}	8.37×10^{-10}		Compernolle et al. 2011[73]
		4.30×10^{-8}	3.10×10^{-8}	3.10×10^{-8}		Huisman et al. 2013[26]
		1.60×10^{-7}	1.15×10^{-7}	1.15×10^{-7}	311	Huisman et al. 2013[26]
"6"	1,2,6-hexanetriol	1.16×10^{-4}	2.50×10^{-6}	2.50×10^{-6}	298	this study
		3.82×10^{-4}	1.16×10^{-4}	1.39×10^{-4}		our CRDS study

function of mole fraction or mass fraction of solute can be arrived at from experimental data and pure component densities. Examples of this approach are shown in Figure 6 for aqueous solutions of sodium chloride and glutaric acid. The solute and solution densities are parametrized in terms of the mfs adopting a similar treatment to previously used for inorganic salt solutions.[62]

$$\rho_{solution} = A_0 + A_1(\mathrm{mfs})^{1/2} + A_2(\mathrm{mfs})^1 + A_3(\mathrm{mfs})^{3/2} + A_4(\mathrm{mfs})^2 \quad (9)$$

The fit must ideally be constrained to the pure component density of the solute in the liquid phase, a thermodynamically unstable phase for both sodium chloride and glutaric acid at room temperature. For inorganic salts, we use the approach adopted by Clegg et al.[62] to estimate the density of the melt at room temperature, defining accurately the value of the density at an mfs of 1. For organic solutes, three possible approaches can be used for treating the density of the pure solute. The fit can be constrained at an mfs of 1 to the crystalline value, to an estimate from the method of Girolami for a subcooled liquid,[63] or can be unconstrained and extrapolated from a fit to the measured densities of water and subsaturated aqueous solutions at low mfs.

The fitted parametrizations for the densities of aqueous solutions of sodium chloride and glutaric acid are shown in Figures 6a and 6c along with the refractive indices then estimated from the molar refraction mixing rules in Figures 6b and 6d. In Figure 6a, the compositional dependence of the density of aqueous sodium chloride represented by eq 9 compares well with the previous measurements and literature parametrizations. In Figure 6c, the use of the crystalline value for the density of the pure solute provides an upper limit for the estimation of the solution density and the method of Girolami provides a lower limit. A fit of eq 9 to the subsaturated data alone provides an intermediate trend. Additionally, we will

DOI: 10.1021/jp510525r
J. Phys. Chem. A 2015, 119, 704−718

consider below the sensitivity of the analysis to this unconstrained fit including an uncertainty in the pure solute density that is ±2.5% from the unconstrained best fit value, the gray envelope in Figure 6c. Notably, the uncertainty associated with the Girolami predictions leads to values that compare adequately within the level of uncertainty associated with the unconstrained fit. Overall, the range of solution density treatments leads to a considerable uncertainty in the estimation of the solution composition from the refractive index when all three methods for the treatment of the pure solute density are compared. This is evident from the spread in retrieved compositions that could be expected by considering the possible range of compositions that would give a mixture of the same refractive index when the mass fraction of solute is >0.6 in Figure 6d. The refractive index of the pure solute is inferred from an extrapolation to solution phase data in the same way as the density of the pure solute.

From a measurement of the refractive index of a binary solution droplet, inferring the composition is straightforward once a particular value for the pure solute density, and thus the parametrization, is assumed. Again, it is important to note that the only parameters needed for the estimation of the refractive index of a solution of any composition are the refractive indices of the pure solutes and water, and a parametrization of the composition-dependent density. The sensitivity of the vapor pressure and hygrosopicity measurements that follow from the uncertainties in the density treatment will be considered in the following section. We will consider a fuller evaluation of the molar refraction mixing rule and sensitivities to pure component densities and refractive indices in a subsequent publication.

5.3. Measurements of Aerosol Hygroscopicity and Component Vapor Pressures. Having established the correlational framework for interpreting measurements of evolving particle size and refractive index and the approach for estimating the solute molarity from the refractive index, we now turn to measurements of hygroscopicity and component vapor pressures. Specifically we consider a homologous series of dicarboyxlic acids (oxalic, malonic, succinic, and glutaric acids), citric acid, glycerol, maleic acid, and 1,2,6-hexanetriol, providing a varied sequence of benchmark compounds of wide ranging hygrosopicity and vapor pressure. We present the data for citric acid and malonic acid in Figures 7−10, showing time series of RH, size, refractive index, and composition and correlational plots for both systems. In each case, the gray envelope on the estimated composition (Figures 7 and 9) shows the sensitivity of the compositional retrieval to the ±2.5% uncertainty in the pure solute density for the solute, using the unconstrained fit to the bulk phase data (the gray envelope in Figure 6). The correlational plots (Figures 8 and 10) are color coded for composition using the scale denoted in the appropriate time-dependent data. The change in both gradient and intercept with RH for each system is clear. The response in solute molarity to RH retrieved from the gradients is shown and compared with predictions from UNIFAC-Peng and the isotherm-RK models. Notably, the limiting constraint in interpreting the measurements remains the uncertainty in the RH measurement, a common factor in all such measurements, and it is not possible to determine which model is more accurate.[13,47]

In Figures 8 and 10 we also indicate the uncertainty in the hygroscopic growth curves resulting from the systematic uncertainty in the trend in refractive index with solution composition arising from uncertainties in the pure solute density. We have chosen to show only the sensitivity arising from the unconstrained fit of the density with a ±2.5% systematic shift in the value of the pure solute density, indicated by the error bar in the solute concentration. More specifically, we show the sensitivity of the hygroscopicity curves inferred from measurements to the three different density treatments for pure malonic, glutaric, and citric acid in Figure 11. If the fit to subsaturated data without unconstraint at the pure solute limit is used to parametrize the solution density, good agreement between measurements and predictions is found for all three systems. When the pure component density is constrained to the value predicted by the Girolami method or the crystalline value, system dependent agreement is observed with significant deviations from the thermodynamic model predictions. This suggests that the unconstrained fit to bulk phase data below the solubility limit provides a good description of the compositional dependence of the solution density. Given that the fit is to a function of the square root of the mass fraction of solute, this strongly weights the low concentration data in defining the shape of the solution density parametrization.

We summarize the pure component vapor pressures estimated for all of the systems studied in Figure 12 and Table 2. The sensitivity of the determination to the thermodynamic treatment used to estimate the activity coefficients and mole fractions at each water activity (eq 3) is also shown with very little change in the estimated pure component vapor pressures between the two models. Notably, the estimated vapor pressures fall within the uncertainty ranges stated in previous determinations published in the literature for all systems apart from maleic acid and 1,2,6-hexanetriol for which the available data is limited. The value for the vapor pressure of citric acid falls between the very large and very small values reported recently by Booth et al.[14] and Huisman et al.[26] for citric acid in a subcooled pure liquid state. The former set of measurements are made using the Knudsen effusion mass spectrometer approach on bulk solid samples and are corrected for the expected dependence on phase with us showing estimated values for the subcooled liquid in Figure 12. Measurements by Huisman et al.[26] were made on single particles using an EDB. The reason for the discrepancies remains unclear. To seek reconciliation of measurements, a range of calibration measurements are required across all techniques to compare and validate the regimes under which vapor pressures can be accurately determined.

6. CONCLUSIONS

Using a new correlational approach for interpreting fluctuations in aerosol droplet size and composition, we report simultaneous measurements of the hygroscopicity and vapor pressure of a range of semivolatile organic compounds with vapor pressures in the range 10^{-2} to 10^{-5} Pa. Unlike conventional measurement strategies that attempt to separate the hygroscopic response from the gas−particle partitioning of the organic component by separating them according to time scale, we have shown that the natural fluctuations and longtime drift in size and refractive index can be used to provide accurate measurements that compare well with past measurements and models. Having presented the framework for these measurements in a previous paper,[18] we provide here a benchmark study over a range of systems encompassing a homologous series of dicarboyxlic acids, citric acid, maleic acid, glycerol, and 1,2,6-hexanetriol. We also consider in detail the estimation of

DOI: 10.1021/jp510525r
J. Phys. Chem. A 2015, 119, 704−718

droplet composition from the refractive index of the droplet and the potential uncertainties in composition, inferred from the cavity enhanced Raman scattering measurement. We have concluded that the molar refraction mixing rule provides an accurate method of retrieving the composition, provided the pure component density of the organic component is known in the pure liquid state or can be estimated from a fit to subsaturated data. In addition, we consider the inherent uncertainties in measurements of component vapor pressures from conventional approaches that report only the evolving size of aerosol droplets, which strongly indicate the advantages in simultaneous measurements of droplet composition (through refractive index) for an accurate determination of component vapor pressures.

So far, we have only considered the use of the correlational framework in the examination of the hygroscopic response and vapor pressures of binary component droplets containing water and a single solute. In subsequent work, we shall extend this approach to study the properties of more complex mixtures of inorganic and organic solutes. In addition, the accuracy of the approach remains limited by the accuracy with which the relative humidity in the gas phase can be determined. In principle, a more accurate method would be to use a comparative droplet approach in which we correlate fluctuations in size and composition between pairs of droplets, an extension of some of our previous work. Finally, the treatment of refractive index used here appears to provide an accurate characterization of droplet composition but a wider range of aerosol of differing composition must be studied to more fully assess the accuracy of the molar refraction mixing rule and the treatments of solution density that are commonly used.

■ ASSOCIATED CONTENT

Supporting Information

Further details of the thermodynamic models used and the uncertainties associated with measurements. This material is available free of charge via the Internet at http://pubs.acs.org.

■ AUTHOR INFORMATION

Corresponding Author

*E-mail: j.p.reid@bristol.ac.uk. Tel: +44 117 331 7388.

Notes

The authors declare no competing financial interest.

■ ACKNOWLEDGMENTS

J.P.R. and D.J.S. acknowledge financial support from the EPSRC through the support of a Leadership Fellowship (EP/G007713/1) awarded to J.P.R. C.C. acknowledges support from the China Scholarship Council. C.S.D. was supported by a National Science Foundation Atmospheric and Geospace Sciences Postdoctoral Research Fellowship during a portion of this work.

■ REFERENCES

(1) Duplissy, J.; DeCarlo, P. F.; Dommen, J.; Alfarra, M. R.; Metzger, A.; Barmpadimos, I.; Prevot, A. S. H.; Weingartner, E.; Tritscher, T.; Gysel, M.; et al. Relating hygroscopicity and composition of organic aerosol particulate matter. *Atmos. Chem. Phys.* **2011**, *11*, 1155−1165.

(2) Hallquist, M.; Wenger, J. C.; Baltensperger, U.; Rudich, Y.; Simpson, D.; Claeys, M.; Dommen, J.; Donahue, N. M.; George, C.; Goldstein, A. H.; et al. The formation, properties and impact of secondary organic aerosol: current and emerging issues. *Atmos. Chem. Phys.* **2009**, *9*, 5155−5236.

(3) Laj, P.; Klausen, J.; Bilde, M.; Plab-Duelmer, C.; Pappalardo, G.; Clerbaux, C.; Baltensperger, U.; Hjorth, J.; Simpson, D.; Reimann, S.; et al. Measuring atmospheric composition change. *Atmos. Environ.* **2009**, *43*, 5351−5414.

(4) Swietlicki, E.; Hansson, H.-C.; Hadmeri, K.; Svenningsson, B.; Massling, A.; McFiggans, G.; McMurry, P. H.; Petadjad, T.; Tunved, P.; Gysel, M.; et al. Hygroscopic properties of sub-micrometer atmospheric aerosol particles measured with H-TDMA instruments in various environments—A review. *Tellus* **2008**, *60*, 432−469.

(5) Ruehl, C. R.; Chuang, P. Y.; Nenes, A. Aerosol hygroscopicity at high (99 to 100%) relative humidities. *Atmos. Chem. Phys.* **2010**, *10*, 1329−1344.

(6) Suda, S. R.; Petters, M. D. Accurate determination of aerosol activity coefficients at relative humidities up to 99% using the hygroscopicity tandem differential mobility analyzer technique. *Aerosol Sci. Technol.* **2013**, *47*, 991−1000.

(7) Zardini, A. A.; Sjogren, S.; Marcolli, C.; Krieger, U. K.; Gysel, M.; Weingartner, E.; Baltensperger, U.; Peter, T. A combined particle trap/HTDMA hygroscopicity study of mixed inorganic/organic aerosol particles. *Atmos. Chem. Phys.* **2008**, *8*, 5589−5601.

(8) Donahue, N. M.; Robinson, A. L.; Stanier, C. O.; Pandis, S. N. Coupled partitioning, dilution, and chemical aging of semi-volatile organics. *Environ. Sci. Technol.* **2006**, *40*, 2635−2643.

(9) Pankow, J. F. Gas/particle partitioning of neutral and ionizing compounds to single and multi-phase aerosol particles.1.Unified modeling framework. *Atmos. Environ.* **2003**, *37*, 3323−3333.

(10) Topping, D. O.; Barley, M. H.; McFiggans, G. The sensitivity of Secondary Organic Aerosol component partitioning to the predictions of component properties − Part 2: Determination of particle hygroscopicity and its dependence on "apparent" volatility. *Atmos. Chem. Phys.* **2011**, *11*, 7767−7779.

(11) Connolly, P. J.; Topping, D. O.; Malavelle, F.; McFiggans, G. A parameterisation for the activation of cloud drops including the effects of semi-volatile organics. *Atmos. Chem. Phys.* **2014**, *14*, 2289−2302.

(12) Topping, D.; Connolly, P.; McFiggans, G. Cloud droplet number enhanced by co-condensation of organic vapours. *Nat. Geosci.* **2013**, *6*, 443−446.

(13) Krieger, U. K.; Marcolli, C.; Reid, J. P. Exploring the complexity of aerosol particle properties and processes using single particle techniques. *Chem. Soc. Rev.* **2012**, *41*, 6631−6662.

(14) Booth, A. M.; Barley, M. H.; Topping, D. O.; McFiggans, G.; Garforth, A.; Percival, C. J. Solid state and sub-cooled liquid vapour pressures of substituted dicarboxylic acids using Knudsen Effusion Mass Spectrometry (KEMS) and Differential Scanning Calorimetry. *Atmos. Chem. Phys.* **2010**, *10*, 4879−4892.

(15) Jennings, S. G.; O'Dowd, C. D.; Cooke, W. F.; Sheridan, P. J.; Cachier, H. Volatility of elemental carbon. *Geophys. Res. Lett.* **1994**, *21*, 1719−1722.

(16) Booth, A. M.; Markus, T.; McFiggans, G.; Percival, C. J.; Mcgillen, M. R.; Topping, D. O. Design and construction of a simple Knudsen Effusion Mass Spectrometer (KEMS) system for vapour pressure measurements of low volatility organics. *Atmos. Meas. Tech.* **2009**, *2*, 355−361.

(17) Zuend, A.; Marcolli, C.; Booth, A. M.; Lienhard, D. M.; Soonsin, V.; Krieger, U. K.; Topping, D. O.; McFiggans, G.; Peter, T.; Seinfeld, J. H. New and extended parameterization of the thermodynamic model AIOMFAC: calculation of activity coefficients for organic-inorganic mixtures containing carboxyl, hydroxyl, carbonyl, ether, ester, alkenyl, alkyl, and aromatic functional groups. *Atmos. Chem. Phys.* **2011**, *11*, 9155−9206.

(18) Cai, C.; Stewart, D. J.; Preston, T. C.; Walker, J. S.; Zhang, Y.-H.; Reid, J. P. A new approach to determine vapour pressures and hygroscopicities of aqueous aerosols containing semi-volatile organic compounds. *Phys. Chem. Chem. Phys.* **2014**, *16*, 3162−3172.

(19) Donahue, N. M.; Chuang, W. K.; Epstein, S. A.; Kroll, J. H.; Worsnop, D. R.; Robinson, A. L.; Adams, P. J.; Pandis, S. N. Why do organic aerosols exist? Understanding aerosol lifetimes using the two-dimensional volatility basis set. *Environ. Chem.* **2013**, *10*, 151−157.

DOI: 10.1021/jp510525r
J. Phys. Chem. A 2015, 119, 704−718

(20) Murphy, B. N.; Donahue, N. M.; Fountoukis, C.; Dall'Osto, M.; O'Dowd, C.; Kiendler-Scharr, A.; Pandis, S. N. Functionalization and fragmentation during ambient organic aerosol aging: application of the 2-D volatility basis set to field studies. *Atmos. Chem. Phys.* **2012**, *12*, 10797−10816.
(21) Chacon-Madrid, H. J.; Murphy, B. N.; Pandis, S. N.; Donahue, N. M. Simulations of smog-chamber experiments using the two-dimensional volatility basis set: linear oxygenated precursors. *Environ. Sci. Technol.* **2012**, *46*, 11179−11186.
(22) Donahue, N. M.; Kroll, J. H.; Pandis, S. N.; Robinson, A. L. A two-dimensional volatility basis set − Part 2: Diagnostics of organic-aerosol evolution. *Atmos. Chem. Phys.* **2012**, *12*, 615−634.
(23) Murphy, B. N.; Donahue, N. M.; Fountoukis, C.; Pandis, S. N. Simulating the oxygen content of ambient organic aerosol with the 2-D volatility basis set. *Atmos. Chem. Phys.* **2011**, *11*, 7859−7873.
(24) Donahue, N. M.; Epstein, S. A.; Pandis, S. N.; Robinson, A. L. A two-dimensional volatility basis set: 1. organic-aerosol mixing thermodynamics. *Atmos. Chem. Phys.* **2011**, *11*, 3303−3318.
(25) Lane, T. E.; Donahue, N. M.; Pandis, S. N. Simulating secondary organic aerosol formation using the volatility basis-set approach in a chemical transport model. *Atmos. Environ.* **2008**, *42*, 7439−7451.
(26) Huisman, A. J.; Krieger, U. K.; Zuend, A.; Marcolli, C.; Peter, T. Vapor pressures of substituted poly-carboxylic acids are much lower than previously reported. *Atmos. Chem. Phys.* **2013**, *10*, 1329−1344.
(27) Barley, M.; Topping, D. O.; Jenkin, M. E.; McFiggans, G. Sensitivities of the absorptive partitioning model of secondary organic aerosol formation to the inclusion of water. *Atmos. Chem. Phys.* **2009**, *9*, 2919−2932.
(28) Barley, M. H.; McFiggans, G. The critical assessment of vapour pressure estimation methods for use in modelling the formation of atmospheric organic aerosol. *Atmos. Chem. Phys.* **2010**, *10*, 749−767.
(29) Cappa, C. D.; Lovejoy, E. R.; Ravishankara, A. R. Determination of evaporation rates and vapor pressures of very low volatility compounds: a study of the C_4-C_{10} and C_{12} dicarboxylic acids. *J. Phys. Chem. A* **2007**, *111*, 3099−3109.
(30) Cappa, C. D.; Lovejoy, E. R.; Ravishankara, A. R. Evidence for liquid-like and non-ideal behavior of a mixture of organic aerosol components. *Proc. Natl. Acad. Sci. U.S.A.* **2008**, *105*, 18687−18691.
(31) Bones, D. L.; Reid, J. P.; Lienhard, D. M.; Krieger, U. K. Comparing the mechanism of water condensation and evaporation in glassy aerosol. *Proc. Natl. Acad. Sci. U.S.A.* **2012**, *109*, 11613−11618.
(32) Shiraiwa, M.; Seinfeld, J. H. Equilibration timescale of atmospheric secondary organic aerosol partitioning. *Geophys. Res. Lett.* **2012**, *39*, 24801.
(33) Riipinen, I.; Pierce, J. R.; Yli-Juuti, T.; Nieminen, T.; Häkkinen, S.; Ehn, M.; Junninen, H.; Lehtipalo, K.; Petäjä, T.; Slowik, J.; et al. Organic condensation: a vital link connecting aerosol formation to cloud condensation nuclei (CCN) concentrations. *Atmos. Chem. Phys.* **2011**, *11*, 3865−3878.
(34) Riipinen, I.; Yli-Juuti, T.; Pierce, J. R.; Petaja, T.; Worsnop, D. R.; Kulmala, M.; Donahue, N. M. The contribution of organics to atmospheric nanoparticle growth. *Nat. Geosci.* **2012**, *5*, 453−458.
(35) Fredenslund, A.; Jones, R. L.; Prausnitz, J. M. Group-contribution estimation of activity coefficients in nonideal liquid mixtures. *AIChE J.* **1975**, *21*, 1086−1099.
(36) Wittig, R.; Lohmann, J.; Gmehling, J. Vapor-Liquid equilibria by UNIFAC group contribution. 6. Revision and Extension. *Ind. Eng. Chem. Res.* **2003**, *42*, 183−188.
(37) Peng, C.; Chan, M. N.; Chan, C. K. The hygroscopic properties of dicarboxylic and multifunctional acids: measurements and UNIFAC predictions. *Environ. Sci. Technol.* **2001**, *35*, 4495−4501.
(38) Wexler, A. S.; Clegg, S. L. J. Atmospheric aerosol models for systems including the ions H^+, NH_4^+, Na^+, SO_4^{2-}, NO_3^-,Cl^-, Br^-, and H_2O. *Geophys. Res.* **2002**, *107*, 4207. See http://www.aim.env.uea.ac.uk/aim/aim.php.
(39) Clegg, S. L.; Seinfeld, J. H.; Brimblecombe, P. Thermodynamic modelling of aqueous aerosols containing electrolytes and dissolved organic compounds. *J. Aerosol Sci.* **2001**, *32*, 713−738.
(40) Zuend, A.; Marcolli, C.; Luo, B. P.; Peter, T. A thermodynamic model of mixed organic-inorganic aerosols to predict activity coefficients. *Atmos. Chem. Phys.* **2008**, *8*, 4559−4593.
(41) Clegg, S. L.; Seinfeld, J. H. Thermodynamic models of aqueous solutions containing inorganic electrolytes and dicarboxylic acids at 298.15 K. 1. The acids as non-dissociating components. *J. Phys. Chem. A* **2006**, *110*, 5692−5717.
(42) McGlashan, M. L. Deviations from Raoult's law. *J. Chem. Educ.* **1963**, *40*, 516.
(43) Dutcher, C. S.; Ge, X.; Wexler, A. S.; Clegg, S. L. Statistical mechanics of multilayer sorption: extension of the Brunauer-Emmett-Teller (BET) and Guggenheim-Anderson-de Boer (GAB) adsorption isotherms. *J. Phys. Chem. C* **2011**, *115*, 16474−16487.
(44) Dutcher, C. S.; Ge, X.; Wexler, A. S.; Clegg, S. L. An isotherm-based thermodynamic model of multicomponent aqueous solutions, applicable over the entire concentration range. *J. Phys. Chem. A* **2013**, *117*, 3198−3213.
(45) Pope, F. D.; Tong, H.-J.; Dennis-Smither, B. J.; Griffiths, P. T.; Clegg, S. L.; Reid, J. P.; Cox, R. A. Studies of single aerosol particles containing malonic acid, glutaric acid, and their mixtures with sodium chloride. II. Liquid-State vapor pressures of the acids. *J. Phys. Chem. A* **2010**, *114*, 10156−10165.
(46) Miles, R. E. H.; Walker, J. S.; Burnham, D. R.; Reid, J. P. Retrieval of the complex refractive index of aerosol droplets from optical tweezers measurements. *Phys. Chem. Chem. Phys.* **2012**, *14*, 3037−3047.
(47) Walker, J. S.; Wills, J. B.; Reid, J. P.; Wang, L.; Topping, D. O.; Butler, J. R.; Zhang, Y.-H. Direct comparison of the hygroscopic properties of ammonium sulfate and sodium chloride aerosol at relative humidities approaching saturation. *J. Phys. Chem. A* **2010**, *114*, 12682−12691.
(48) Preston, T. C.; Reid, J. P. Accurate and efficient determination of the radius, refractive index, and dispersion of weakly absorbing spherical particle using whispering gallery modes. *J. Opt. Soc. Am. B* **2013**, *30*, 2113−2122.
(49) Carruthers, A. E.; Walker, J. S.; Casey, A.; Orr-Ewing, A. J.; Reid, J. P. Selection and characterization of aerosol particle size using a bessel beam optical trap for single particle analysis. *Phys. Chem. Chem. Phys.* **2012**, *14*, 6741−6748.
(50) Cotterell, M. I.; Mason, B. J.; Carruthers, A. E.; Walker, J. S.; Orr-Ewing, A. J.; Reid, J. P. Measurements of the evaporation and hygroscopic response of single fine-mode aerosol particles using a Bessel beam optical trap. *Phys. Chem. Chem. Phys.* **2014**, *16*, 2118−2128.
(51) Davies, J. F.; Haddrell, A. E.; Reid, J. P. Time-resolved measurements of the evaporation of volatile components from single aerosol droplets. *Aerosol Sci. Technol.* **2012**, *46*, 666−677.
(52) Ray, A. K.; Davis, E. J.; Ravindran, P. Determination of ultralow vapor pressures by submicron droplet evaporation. *J. Chem. Phys.* **1979**, *71*, 582−587.
(53) Constantinou, L.; Gani, R. New group contribution method for estimating properties of pure compounds. *AIChE J.* **1994**, *40*, 1697−1710.
(54) Reid, R. C.; Prausnitz, J. M.; Poling, B. E. *The Properties of Gases and Liquids*; McGraw-Hill: New York, 1987.
(55) Nannoolal, Y.; Rarey, J.; Ramjugernath, J. Estimation of pure component properties Part 2. Estimation of critical property data by group contribution. *Fluid Phase Equilib.* **2007**, *252*, 1−27.
(56) Jankowski, M. D.; Henry, C. S.; Broadbelt, L. J.; Hatzimanikatis, V. Group contribution method for thermodynamic analysis of complex metabolic networks. *Biophys. J.* **2008**, *95*, 1487−1499.
(57) Mavrovouniotis, M. L. Estimation of standard Gibbs energy changes of biotransformation. *J. Biol. Chem.* **1991**, *266*, 14440−14445.
(58) Mavrovouniotis, M. L. Group contributions for estimating standard Gibbs energies of formation of biochemical compounds in aqueous solution. *Biotechnol. Bioeng.* **1990**, *36*, 1070−1082.
(59) Wills, J. B.; Butler, J. R.; Palmer, J.; Reid, J. P. Using optical landscapes to control, direct and isolate aerosol particles. *Phys. Chem. Chem. Phys.* **2009**, *11*, 8015−8020.

DOI: 10.1021/jp510525r
J. Phys. Chem. A 2015, 119, 704−718

(60) Mitchem, L.; Reid, J. P. Optical manipulation and characterisation of aerosol particles using a single-beam gradient force optical trap. *Chem. Soc. Rev.* **2008**, *37*, 756−769.
(61) Liu, Y.; Daum, P. H. Relationship of refractive index to mass density and self-consistency of mixing rules for multicomponent mixtures like ambient aerosols. *J. Aerosol Sci.* **2008**, *39*, 974−986.
(62) Clegg, S. L.; Wexler, A. S. Densities and apparent molar volumes of atmospherically important electrolyte solutions. 1. The solutes H_2SO_4, HNO_3, HCl, Na_2SO_4, $NaNO_3$, NaCl, $(NH_4)_2SO_4$, NH_4NO_3, and NH_4Cl from 0 to 50 C, including extrapolations to very low temperature and to the pure liquid state, and $NaHSO_4$, NaOH, and NH_3 at 25 C. *J. Phys. Chem. A* **2011**, *115*, 3461−3474.
(63) Girolami, G. S. A simple "Back of the envelope" method for estimating the densities and molecular volumes of liquids and solids. *J. Chem. Educ.* **1994**, *71*, 962.
(64) Tang, I. N.; Tridico1, A. C.; Fung, K. H. Thermodynamic and optical properties of sea salt aerosol. *J. Geophys. Res.* **1997**, *D19*, 23269−23275.
(65) Riipinen, I.; Koponen, I. K.; Frank, G. P.; Hyvadrinen, A.-P.; Vanhanen, J.; Lihavainen, H.; Lehtinen, K. E. J.; Bilde, M.; Kulmala, M. Adipic and malonic acid aqueous solutions: Surface tensions and saturation vapor pressures. *J. Phys. Chem. A* **2007**, *111*, 12995−13002.
(66) Soonsin, V.; Zardini, A. A.; Marcolli, C.; Zuend, A.; Krieger, U. K. The vapor pressures and activities of dicarboxylic acids reconsidered: the impact of the physical state of the aerosol. *Atmos. Chem. Phys.* **2010**, *10*, 11753−11767.
(67) Koponen, I. K.; Riipinen, I.; Hienola, A.; Kulmala, M.; Bilde, M. Thermodynamic properties of malonic, succinic, and glutaric acids: evaporation rates and saturation vapor pressures. *Environ. Sci. Technol.* **2007**, *41*, 3926−3933.
(68) Bilde, M.; Pandis, S. N. Evaporation rates and vapor pressures of individual aerosol species formed in the atmospheric oxidation of α- and β-Pinene. *Environ. Sci. Technol.* **2001**, *35*, 3344−3349.
(69) da Silva, M. A. R.; Monte, M. J.; Ribeiro, J. R. Vapour pressures and the enthalpies and entropies of sublimation of five dicarboxylic acids. *J. Chem. Thermodyn.* **1999**, *31*, 1093−1107.
(70) Lide, D. R.; *CRC Handbook of Chemistry and Physics*, 44th ed.; Chemical Rubber Company: Boca Raton, FL, 1962.
(71) Winstrom, L. O.; Kulp, L. Vapor pressure of maleic anhydride. *Ind. Eng. Chem.* **1949**, *41*, 2584−2586.
(72) Yaws, C. L.; Narasimhan, P. K.; Gabbula, C. *Handbook of Antoine Coefficients for Vapor Pressure*; Knovel: New York, 2009.
(73) Compernolle, S.; Ceulemans, K.; Muller, J. EVAPORATION: a new vapour pressure estimation method for organic molecules including non-additivity and intramolecular interactions. *Atmos. Chem. Phys.* **2011**, *11*, 9431−9450.

DOI: 10.1021/jp510525r
J. Phys. Chem. A 2015, 119, 704−718